Polymer 51 (2010) 5462–5472

Contents lists available at ScienceDirect

Polymer

journal homepage: www.elsevier.com/locate/polymer

Isothermal crystallization of lightly sulfonated syndiotactic polystyrene/montmorillonite clay nanocomposites

Sonya D. Benson, Robert B. Moore*

Department of Chemistry, Macromolecules and Interfaces Institute, Virginia Polytechnic Institute and State University, Blacksburg, VA 24061, United States

ARTICLE INFO

Article history:
Received 22 July 2010
Received in revised form
8 September 2010
Accepted 12 September 2010
Available online 18 September 2010

Keywords:
Ionomer
Clay nanocomposite
Isothermal crystallization

ABSTRACT

Lightly sulfonated syndiotactic polystyrene (sPS) nanocomposites were prepared using a solution intercalation technique, and the effect of montmorillonite clay on the crystallization kinetics of sulfonated sPS ionomer nanocomposites was systematically studied. Wide angle X-ray diffraction (WAXD) and transmission electron microscopy (TEM) were used to evaluate the dispersion of clay platelets within sPS and sulfonated sPS ionomer (SsPS) matrices. Experimental results obtained from WAXD and TEM revealed a predominately exfoliated morphology within the SsPS ionomer containing 5 wt.% of organically-modified clay. The corresponding non-sulfonated sPS control exhibited a mixed morphological structure consisting of intercalated platelets and many platelets that were present as micron-sized agglomerates. Using differential scanning calorimetry (DSC), the Avrami approach was used to elucidate information related to nucleation and growth within the sPS and SsPS systems during the isothermal crystallization process. Pristine and organically-modified clays significantly increased the overall crystallization rate of the SsPS ionomer, while the nanoclays slightly decreased the crystallization rate of the non-ionic sPS. The mechanistic origins of increased crystallization rates within the SsPS ionomer clay nanocomposites were attributed to multiple phenomena including disruption of the ionomer electrostatic network and a nucleating effect due to the presence of well-separated, homogeneously dispersed clay platelets.

1. Introduction

Polymer/clay nanocomposites are very important materials from an industrial perspective due to the potential material property enhancements that can be realized with only a small addition of properly dispersed nanoscale clay platelets [1,2]. Therefore, a significant amount of research has been focused on the preparation of polymer/clay nanocomposites using industrially important semicrystalline polymers such as polypropylene [3,4], polyethylene [5,6], polyesters [7–10], polyamides [11,12], and syndiotactic polystyrene [13–23]. However, the organophillic character of many industrially important semicrystalline polymers prevents sufficient interaction between the polymer and clay resulting in poor dispersion of the naturally polar aluminosilicate clay within the hydrophobic polymer matrix.

Ion-containing polymers (specifically, ionomers containing less than ca. 10 mol% ionic functionality along the chains) have been investigated as the host matrix for the preparation of polymer/clay nanocomposites [24,25] and as compatibilizers between a host matrix and clay platelets as well [26–28]. The advantage of utilizing ionomers as matrices and compatibilizers in polymer/clay nanocomposites originates from strong specific interactions that can occur between the ionic groups of the ionomer and the highly charged, polar clay surface. The improved interaction between the ion-containing polymer and polar clay through favorable electrostatic interactions may facilitate the development of intercalated and exfoliated morphologies. The resultant intercalated and exfoliated morphologies reveal and expose the high clay surface area necessary to realize enhanced mechanical, thermal, and barrier properties [24,25].

Initial demonstration of the effectiveness of ionomers as host matrices for the preparation of polymer nanocomposites was provided by Chisholm et al. [24]. This study revealed that incorporation of as little as 1.0 mol% $-SO_3Na$ groups onto poly(butylene terepthalate) (PBT) resulted in the formation of an exfoliated morphology of organically-modified montmorillonite clay platelets that were well-dispersed throughout the PBT ionomer matrix. Polyester ionomer clay nanocomposites have also been prepared using poly(ethylene terepthalate) (PET) containing up to 5.8 mol% sodium sulfonate ionic groups [25]. Barber et al. have shown that

* Corresponding author. Tel.: +1 540 231 0641; fax: +1 540 231 8517.
E-mail address: rbmoore3@vt.edu (R.B. Moore).

0032-3861/$ – see front matter © 2010 Elsevier Ltd. All rights reserved.
doi:10.1016/j.polymer.2010.09.024

incorporation of low levels of sodium sulfonate groups into PET along with the utilization of organically-modified montmorillonite clay results in the formation of highly intercalated and exfoliated ionomer clay structures. This study using PET ionomers, supported the previous work completed by Chisholm and coworkers using PBT ionomers and further demonstrated that ionomers may be used as matrices to create intercalated and exfoliated polymer nanocomposites.

Since the initial work of Chisholm et al., further research has been conducted using ionomers as host matrices for the development of polymer nanocomposites. Nanocomposites have been prepared using ionomers based on polypropylene, polyethylene [29], and polystyrene [30]. Important aspects of ionomer nanocomposite preparation have been investigated such as the effects of ionic functionality on clay platelet dispersion [25], the effects of melt processing on the degree of exfoliation [31], and the effect of surfactant structure [32] on the ionomer nanocomposite morphology. However, in order for semicrystalline ionomer nanocomposites to be effectively used in industrial and commercial applications, a detailed understanding of the effect of clay on the crystallization behavior of the ionomer matrix is of fundamental importance.

Our initial ionomer nanocomposite studies [24,25] provided information on the effect of tactoid, intercalated, and exfoliated morphological clay arrangements on the crystallization behavior of polyester ionomers. However, conflicting information was obtained from the study of the polyester based ionomer nanocomposites systems based upon poly(ethylene terepthalate) and poly(butylene terepthalate). It was found that the crystallization half-time (the time required for the material to reach 50% crystallinity during isothermal crystallization) slightly increased for PBT ionomer nanocomposites. The increase in crystallization half-time suggested the overall rate of bulk crystallization is decreased and clay did not act as a nucleating agent within the PBT ionomer matrix. Moreover, isothermal crystallization data of PBT ionomer nanocomposites revealed the crystallization half-time was not dependent upon the morphological state of the dispersed clay particles. In contrast, Barber et al. [25] found the crystallization behavior of PET ionomer nanocomposites to be dependent upon the degree of clay exfoliation within the ionomer matrix. The crystallization half-time of PET ionomer nanocomposites increased with increasing degree of clay exfoliation indicating the exfoliated nanoscale platelets are less effective nucleants relative to micron-sized clay tactoids.

Due to the contrasting effect of clay on the crystallization kinetics and behavior of semicrystalline PBT and PET ionomers, it necessary to further study the effect of clay on the crystallization behavior and kinetics of a *model* semicrystalline ionomer. Sulfonated syndiotactic polystyrene (SsPS) has been utilized as a model semicrystalline ionomer in fundamental investigations studying the link between ionic aggregation and crystallization behavior of ionomers [33–36]. Since the ionic species of SsPS are incorporated through a post-polymerization sulfonation reaction and not through copolymerization (as with previous studies), varying the ionic content does not significantly disrupt the microstructure and molecular weight distribution of the resulting SsPS copolymer. Additionally, a significant advantage of utilizing SsPS as a model semicrystalline ionomer results from the high stereoregularity of sPS, which allows it to crystallize rapidly from the melt. The wealth of fundamental information on the crystallization behavior of sulfonated sPS provided by these studies renders it a prime candidate for a detailed study of the effect of clay on the crystallization behavior and kinetics of semicrystalline ionomers in general.

In a previous study, the preparation and characterization of SsPS nanocomposite morphology has been reported as a function of ionic content and neutralizing counterion [37]. It was shown that the degree of clay exfoliation increased with increasing ionic content and with increasing size of the neutralizing counterion. This study provided initial qualitative observations on the non-isothermal crystallization behavior of SsPS nanocomposites by monitoring the peak crystallization temperature on cooling from the melt. However, a more detailed quantitative study of the effect of clay on the crystallization behavior and kinetics of SsPS is needed to gain further insight into the possible mechanism of crystallization of the SsPS ionomer in the presence of montmorillonite clay. Thus, the purpose of this study is to determine the effect of pristine and organically-modified clay on the morphology, crystallization behavior, and isothermal crystallization kinetics of SsPS, a model semicrystalline ion-containing polymer.

2. Experimental

2.1. Materials

Syndiotactic polystyrene (Questra 102) MW of 310,000 g/mol was donated by the Dow Chemical Company. Reagent grade chloroform, 1,1,2-trichlorobenzene (TCB), methanol, sulfuric acid, and potassium monopthalate were obtained from Fisher Scientific. Hexanoic anhydride and cesium hydroxide were received from Sigma Aldrich. Cloisite® Na^+ and Cloisite® 10A were donated by Southern Clay Products. The clays were used in the received state without additional drying. The cation exchange capacities for Cloisite® Na^+ and Cloisite® 10A are 92.6 and 125 and milli-equivalents/100 g, respectively. The organic modification agent for Cloisite® 10A is a quaternary amine salt consisting of a dimethylbenzyl, hydrogenated tallow. The hydrogenated tallow is made up of ~65% C18, ~30% C16, and ~5% C14 chains. Cloisite®10A has been shown to produce intercalated and exfoliated nanostructures in many styrenated polymer matrices [13,38–41] and is thus a proper choice for enhancing polymer clay interactions in the sPS matrix. Cloisite® Na^+ and Cloisite® 10A will be identified as Na^+MMT and OMMT respectively. The clay organic modification agent, Arquad DMHTB-80E was donated by Akzo Nobel Surface Chemistry, LLC.

2.2. Sulfonation of syndiotactic polystyrene

Previous differential scanning calorimetry (DSC) investigations of SsPS ionomers have identified the effect of the degree of sulfonation on the crystallization behavior of SsPS [34]. It has been demonstrated that incorporating greater than 2.0 mol% of ionic content within sPS drastically inhibits the ability of sPS to crystallize. Therefore, we have chosen to lightly sulfonate sPS to yield an ion-containing polymer with 1 mol% sulfonation. By introducing 1 mol% sulfonate groups, the crystallization kinetics of SsPS occurs on a readily observable timescale at crystallization temperatures similar to that of the sPS homopolymer. Thus, direct comparisons between the behavior of the SsPS ionomer and the sPS homopolymer can be made.

The sulfonation agent was prepared according to previously published procedures [34] using chloroform as the solvent. Chloroform (25 mL) was added to a 50 mL volumetric flask containing 0.03 mol of hexanoic anhydride. The chloroform/hexanoic anhydride solution was cooled in an ice bath for 1 h, and then 1 mL of concentrated sulfuric acid was added to the chilled solution and shaken vigorously. Additional chloroform was added to the volumetric flask to the 50 mL mark.

sPS was dissolved in chloroform at 100 °C for 1.5 h in a PARR pressure reactor to yield a 2.5% w/v solution. After 1.5 h, the solution was cooled to 70 °C and then transferred to a three-neck round bottom flask. Additional chloroform was added to yield a 1% w/v sPS solution. The sPS solution was allowed to equilibrate at 70 °C

under a nitrogen purge. After equilibration, the appropriate amount of sulfonating reagent was added and the reaction was allowed to proceed for 1 h at 70 °C under a nitrogen purge. After 1 h, 10 mL methanol was added to the solution to terminate the reaction. The solution was poured into a large excess of methanol to precipitate the polymer. The precipitated polymer was filtered and washed with deionized water. The resulting polymer was dried under vacuum at 100 °C for 12 h. The vacuum dried ionomer was redissolved in chloroform using a PARR pressure reactor for 1.5 h at 100 °C and then steam stripped in deionized water to remove residual sulfonating reagent and solvent. The ionomer was then dried in a vacuum oven at 70 °C for 24 h. The degree of sulfonation was determined by nonaqueous titration with methanolic sodium hydroxide. The methanolic sodium hydroxide was standardized using potassium monopthalate.

2.3. Neutralization of sulfonated syndiotactic polystyrene

The cesium counterion was chosen as the neutralizing counterion for SsPS within this study of the crystallization behavior and kinetics of SsPS nanocomposites based on previous work by Orler et al. [35]. The relatively large cesium counterion yields weaker electrostatic interactions compared to SsPS ionomers neutralized with alkali metals of smaller ionic radii, and thus leading to enhanced crystallization. Due to the presence of these more thermally-labile ionic aggregates, cesium-neutralized SsPS allows crystallization of chain segments to occur on timescale similar to the sPS homopolymer. Therefore, cesium-neutralized SsPS was considered to be the most appropriate SsPS ionomer to study the effect of clay on the crystallization behavior and kinetics of the semicrystalline SsPS.

The SsPS ionomer was completely neutralized using 0.1 M cesium hydroxide. The SsPS was dissolved in chloroform using a PARR pressure reactor at 100 °C for 1.5 h. The appropriate amount of 0.1 M CsOH was added to the SsPS solution to obtain a fully neutralized ionomer. The fully cesium-neutralized SsPS 1.0 mol% ionomer was used as the ionomer matrix within this study and will be identified as SsPS.

2.4. Nanocomposite preparation

Nanocomposites were prepared using the solution intercalation method [1,2]. Dispersions of Na^+MMT and OMMT (0.5% w/v) were prepared by adding the appropriate amount of clay to chloroform. The respective clay/chloroform mixtures were heated under reflux at 60 °C for 24 h with vigorous stirring. After 24 h, the clay dispersions were sonicated for 2 h.

sPS and SsPS nanocomposites containing 1, 3, and 5% w/w of Na^+MMT and OMMT clays were prepared. Solutions of sPS and SsPS were prepared by dissolving the appropriate amount of the homopolymer or the ionomer in chloroform to yield 1.5% w/v solutions. The sPS homopolymer or SsPS ionomer was dissolved in chloroform using a PARR pressure reactor at 100 °C for 1.5 h. The solutions were removed from the reactor upon dissolution and transferred to 50 mL round bottom flasks. The appropriate volume of clay dispersions to yield 1, 3, or 5% w/w of Na^+MMT or OMMT was taken from the previously prepared 0.5% w/v clay dispersions, while the mixture was being vigorously stirred to ensure that a homogeneous sample volume was removed. After adding the appropriate amount of clay dispersion to the dissolved polymer, the samples were allowed to mix with vigorous stirring under reflux for 24 h at 60 °C. After 24 h, the mixtures were dried at RT for 5 days to evaporate the solvent followed by drying in a vacuum oven for 24 h at 60 °C.

2.5. Sulfonated syndiotactic polystyrene containing organic modification agent

In order to isolate the effect of the organic modification agent on the crystallization behavior of SsPS, the organic modification agent used to render the pristine clay more organophilic, DMHTB, was added to solutions of the SsPS ionomer without any clay present. A solution of DMHTB was prepared by dissolving the surfactant in TCB for 1 h under reflux conditions. The appropriate amount of the DMHTB solution was added to 1.5% w/v solutions of SsPS ionomer in TCB to yield the amount of DMHTB surfactant that would be present at Cloisite® 10A contents of 1, 3, and 5 wt.%. The SsPS/DMHTB solutions were mixed with vigorous stirring for 1 h followed by drying in a vacuum oven for 24 h at 60 °C.

2.6. Transmission electron microscopy

Solution-cast samples were prepared for morphological analysis using transmission electron microscopy (TEM) by embedding solution-cast sPS and SsPS clay mixtures into epoxy resin. The epoxy resin used was Spurr's Low Viscosity embedding mixture obtained from Electron Microscopy Sciences. The resin was prepared according the supplier's protocol. The resin containing the nanocomposites samples was dried in vacuum oven at 60 °C for 12 h. The samples were microtomed at room temperature with a diamond knife using a Reichart Ultramicrotome in order to obtain 80 nm thick sections. Microtomed sections were transferred from water onto 200 mesh copper grids and used without staining. The high electron density of the clay platelets provided the necessary contrast for morphological evaluation using TEM. TEM micrographs of solvent-cast sPS and SsPS clay mixtures were obtained using a JEOL 2100 transmission electron microscope operating at 200 kV. The microscope was interfaced with a Gatan camera that was utilized to obtain digital photomicrographs.

2.7. Wide angle X-ray diffraction

Wide angle X-ray diffraction (WAXD) was used as a quantitative tool to determine the changes in clay platelet intergallery height by following changes in the basal spacing of the clay. Solvent-cast nanocomposite samples were ground into a powder using a mortar and pestle prior to WAXD analysis. A Rigaku Ultima III X-ray Diffractometer using Cu K_α radiation ($\lambda = 1.54$ nm) operating at 40 kV and 44 mA was used to obtain nanocomposite WAXD profiles in the 2 theta region from $2\theta = 2–10°$. The WAXD profiles were obtained at a scan rate of 0.1°/min and a step size of 0.05.

2.8. Differential scanning calorimetry

Thermal behavior and crystallization kinetics of the polymer clay mixtures were studied using differential scanning calorimetry (DSC). A Perkin–Elmer DSC-7 was used to probe the thermal behavior of the prepared nanocomposites under isothermal crystallization conditions at 240 °C. The weight for each sample was maintained between 6 and 8 mg. The solution-cast samples will be identified throughout the paper using the following terminology: sPS XNa^+MMT, sPS XOMMT, SsPS XNa^+MMT and SsPS XOMMT where X will equal 0, 1, 3, or 5 wt.% Na^+MMT or OMMT clay in the sPS homopolymer or the SsPS ionomer.

DSC analysis was performed under a continuous nitrogen flow to minimize sample degradation. The samples were heated to 330 °C and held at that maximum temperature for 5 min to erase previous thermal history and the presence of any persistent nuclei. Following a rapid temperature ramp at −200 °C/min, isothermal crystallization was carried out at 240 °C for 60 min. Pyris Perkin–Elmer software

was used to analyze the resulting DSC traces. The crystallization half-time, $t_{½}$, the time at which 50% of the material has crystallized, was obtained from isothermal holds and used as a measure of changes in the bulk crystallization rate of the neat polymers and polymer clay mixtures.

2.9. Polarized light microscopy

The determination of the spherulitic growth rates of the pure matrices and clay containing matrices was carried out using polarized light microscopy. A Nikon LV100 microscope equipped with a Nikon DXM1200 digital camera was used in crossed-polarized configuration to monitor spherulitic growth under isothermal conditions. Images were captured and analyzed using Nikon NIS-Elements BR software. Isothermal crystallization conditions were achieved using a Linkam TMS600 hotstage operated by a Linkam TMS 94 controller and Linkam Linksys32 software. The samples were heated to 330 °C on the Linkam hotstage and held at that maximum temperature for 5 min. Following a rapid temperature ramp at −100 °C/min, isothermal crystallization was carried out at 240 °C with periodic image capture until complete spherulitic impingement occurred.

2.10. Small-angle laser light scattering

Small-angle laser light scattering (SALLS) patterns were obtained in H_v mode using a laser light scattering experimental configuration similar to that of Stein and Rhodes [42]. A 3 mW He–Ne laser light of 632.8 nm (Oriel Corporation, Model 6697) was used as the incident light and the H_v patterns were captured using a SenSys 1401E (Photometrics) CCD camera positioned at a sample-to-detector distance of 380 mm. The spherulite diameters of the pristine polymers and polymer/clay mixtures were obtained using volume-filled samples that were isothermally crystallized at 240 °C using a Linkam hotstage according to the heating profile used for the polarized optical microscopy analysis. The H_v patterns were analyzed using POLAR Software (STAR, State University of New York) to obtain the maximum scattering intensity at an azimuthal angle of 45°.

3. Results and discussion

3.1. Morphological characterization of sPS/SsPS clay nanocomposites

WAXD analysis provides insight into the morphological state of polymer clay mixtures through a determination of the degree of periodicity and order present within the dual component system. Fig. 1A contains WAXD profiles of solvent-cast sPS containing up to 5 wt.%. Na^+MMT. As the concentration of Na^+MMT is increased within the sPS matrix from 1 to 5 wt.% Na^+MMT, noticeable changes in the WAXD patterns occur. The peak attributable to Na^+MMT clay at 6.7° 2θ increases in intensity, broadens in peak breadth, and finally merges with the peak corresponding to the sPS crystalline diffraction peak at 8.0° 2θ [43–45]. The increase in the intensity and breadth of the peak centered at 6.7° 2θ with increasing clay content suggests that there are not sufficient polymer-clay interactions between the hydrophobic sPS homopolymer and the polar aluminosilicate Na^+MMT clay to lead to intercalation or exfoliation.

The WAXD profiles of the SsPS Na^+MMT mixtures are provided in Fig. 1B. There is no peak at 7.0° 2θ corresponding to Na^+MMT in the SsPS 1 wt.% Na^+MMT mixture indicating that Na^+MMT platelets may be exfoliated within the ionomer matrix. However, upon addition of 3 wt.% Na^+MMT into SsPS, a very broad peak appears at 7.0° 2θ. This peak is attributed to unintercalated Na^+MMT. As with the pure sPS matrix, the peak corresponding to Na^+MMT continues to broaden and increase in intensity upon addition of 5 wt.% Na^+MMT into the ionomer matrix. In agreement with our previous work with polyester ionomers [24,25], these data indicate that ionic interactions alone are not sufficient to disrupt the tactoid arrangement of Na^+MMT platelets without organic modification of the clays.

Many investigations into the preparation of polymer nanocomposites have been focused on surfactant modification of the highly charged clay surface in order to render the platelet surface more organophilic and thus aid in the dispersion of the platelets in hydrophobic polymer matrices [46–48]. To facilitate enhanced dispersion of the clay nanoparticles within each polymer matrix,

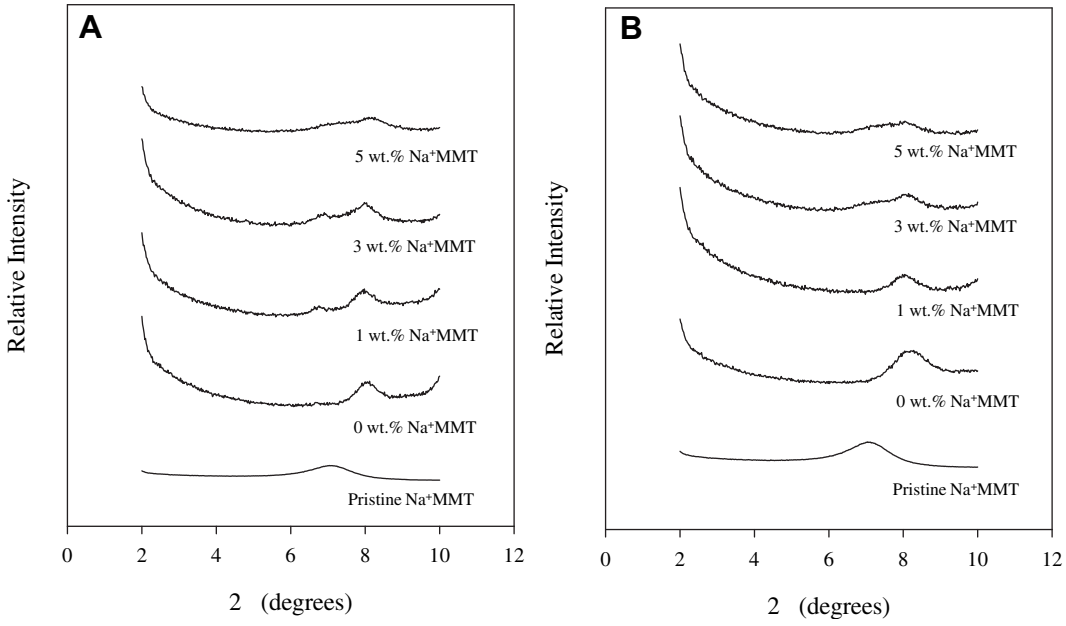

Fig. 1. WAXD patterns in the range of 2θ = 2–10° for (A) sPS Na^+MMT mixtures and (B) SsPS Na^+MMT mixtures.

sodium montmorillonite chemically-modified with a quaternary ammonium surfactant containing a long chain alkyl portion and a benzyl moiety was utilized. In Fig. 2A of sPS OMMT composites, the peak associated with organically-modified clay is present at 4.7° 2θ. The peak attributed to OMMT clay increases in intensity with increasing clay content and does not shift in peak position suggesting that organic modification of the clay alone is not sufficient to produce an exfoliated sPS OMMT nanocomposite.

In distinct contrast to the WAXD data of sPS OMMT mixtures, the WAXD profiles of SsPS containing OMMT show only one diffraction peak located at 8.2° 2θ corresponding to the sPS crystalline form. The most important observation is that the WAXD profiles of SsPS OMMT composites are featureless in the region characteristic of layered OMMT indicating that the OMMT platelets are present in the ionomer matrix in an exfoliated manner. Therefore, it is clear that chemical modification of both polymer (i.e., ionic functionalization) and clay (i.e., organic modification) appears to be very effective in creating a nanocomposite morphology that may consist of highly disordered platelets within the ionomer matrix.

While WAXD is a highly useful technique used to probe the morphology of polymer nanocomposites, WAXD is not sufficient alone to fully characterize the morphology of layered silicate platelets within any polymer matrix. It is often coupled with TEM analysis in order to more fully characterize the state of clay dispersion within the polymeric matrix. Fig. 3A and 3B contain TEM micrographs of solvent-cast sPS and SsPS matrices containing 5 wt.% Na^+MMT, respectively. The TEM micrograph of sPS 5 wt.% Na^+MMT in Fig. 3A reveals a mixed platelet morphology dominated by the presence of large micron-scale clay tactoids. The TEM micrograph of SsPS containing 5 wt.% Na^+MMT in Fig. 3B reveals the presence of micron-sized agglomerates of Na^+MMT platelets within the ionomer matrix and the overall morphology of the SsPS 5 wt.% Na^+MMT mixture is very similar to that of the sPS homopolymer containing 5 wt.% Na^+MMT. In agreement with the WAXD data, this suggests that ionomer-Na^+MMT platelet interactions were not sufficient to result in a highly exfoliated or intercalated platelet morphology.

The morphology of sPS 5 wt.% OMMT as shown in Fig. 4A contains large micron-scale OMMT agglomerates. However, there appears to be evidence of intercalated structures within the sPS 5 wt.% OMMT hybrid and even single platelet features. Coupling TEM micrographs of sPS hybrids containing 5 wt.% Na^+MMT and OMMT with WAXD data suggests that these hybrid materials consist of primarily micro-composite features with a relatively small portion of intercalated platelet stacks.

However, in contrast, Fig. 4B of SsPS 5 wt.% OMMT reveals a drastically different platelet morphology compared to the sPS OMMT mixtures. The OMMT platelets are present as stacks consisting of tens of platelets and single platelet features as well. Furthermore, there are no micron-scale tactoid features present in the SsPS 5 wt.% OMMT nanocomposite. Therefore, based upon TEM and WAXD results, it appears that SsPS-OMMT platelet interactions are sufficient to result in a predominately exfoliated, relatively well-dispersed ionomer- clay nanocomposite.

3.2. Isothermal crystallization of sPS/SsPS clay nanocomposites

The development of crystallinity during isothermal crystallization within each polymer clay system was monitored by applying the following relationship:

$$X_c(t) = \frac{\int_0^t \frac{dH}{dT}\,dt}{\int_0^\infty \frac{dH}{dT}\,dt} \quad (1)$$

The expression given in equation (1) represents the fractional crystallinity of the bulk polymer system, $X_c(t)$, and is equal to the heat evolved during isothermal crystallization at a specific time t divided by the total heat generated during the entire crystallization process. Crystallization half-times ($t_{½}$ values) were determined from isothermal crystallization experiments, defined as the time required to react 50% of the samples maximum crystallinity, and were used as a measure of the rate of bulk isothermal crystallization.

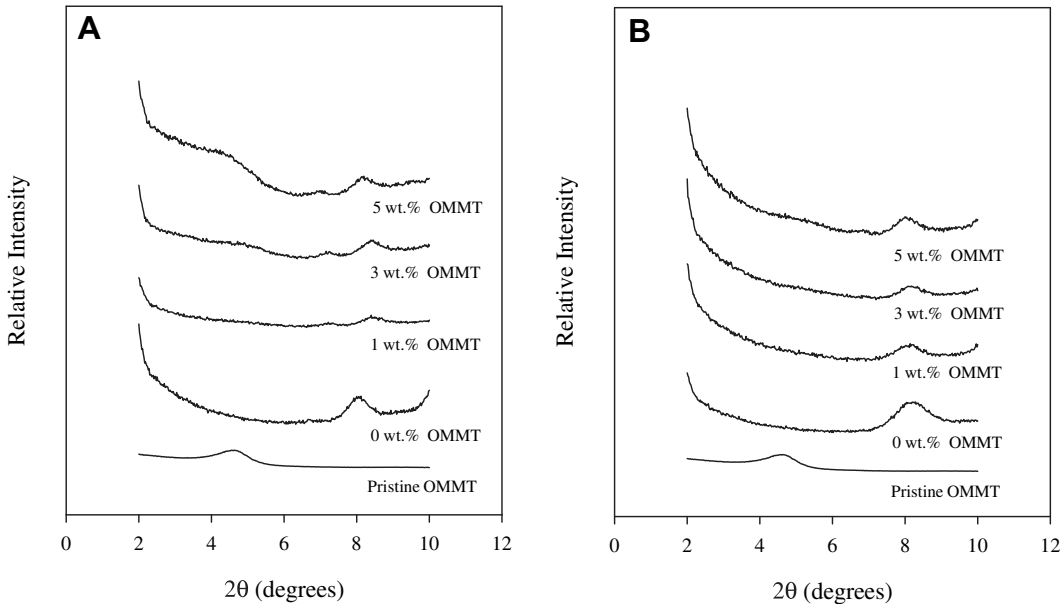

Fig. 2. WAXD patterns in the range of 2θ = 2–10° for (A) sPS OMMT mixtures and (B) SsPS OMMT mixtures.

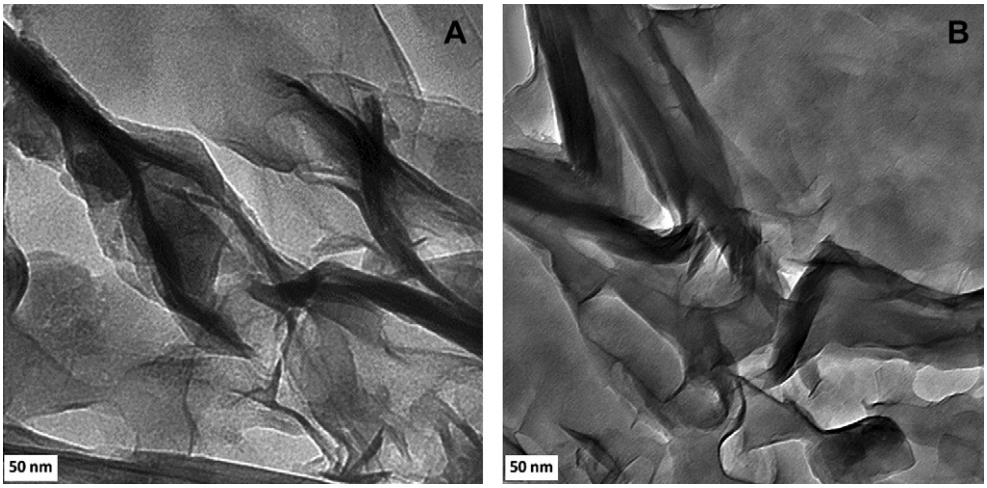

Fig. 3. TEM of (A) sPS 5 wt.% Na^+MMT mixtures and (B) SsPS 5 wt.% Na^+MMT mixtures. The scale bar in each image is 50 nm.

Fig. 5A contains the plot of the fraction of material crystallized $X_c(t)$ versus ln time at 240 °C for sPS Na^+MMT. As the concentration of Na^+MMT increases from 0 to 5 wt.% Na^+MMT within the sPS matrix, each crystallization isotherm shifts to longer times. The increase in the crystallization time with increasing clay content suggests that sPS chain mobility is retarded by the presence of the clay. In studies of sPS containing organically-modified clay, Wu and coworkers [15] determined that low clay concentrations (less than 1 wt.%) induce heterogeneous nucleation within the sPS matrix. However, at concentrations of 5 wt.% of organically-modified clay, Wu and coworkers observed a reduction in the mobility of sPS polymer chains during crystallization despite the occurrence of heterogeneous nucleation. The isothermal crystallization results obtained within this study of sPS clay mixtures is similar to that observed by Wu and coworkers. We also attribute the decrease in the rate of crystallization of sPS nanocomposites to a reduction in polymer mobility in the presence of the clay, and retardation due to rejection of the large tactoids from the crystal growth front [49].

Fig. 5B provides the plot of $X_c(t)$ versus ln time at 240 °C for SsPS containing Na^+MMT. Upon incorporation of 1 and 3 wt.% Na^+MMT, there is a shift of the isotherms to shorter crystallization times. While the overall crystallization rate of these ionomer/clay nanocomposites is significantly slower than that of the pure sPS/clay nanocomposites, this behavior is likely attributed to enhanced nucleation through enhanced electrostatic interactions. For the isothermal crystallization of SsPS 5 wt.% Na^+MMT, however, no additional shift is observed, which suggests that a maximum clay loading limit exists, where ionomer–platelet interactions are maximized and further addition of Na^+MMT platelets may begin to inhibit the crystallization process.

Fig. 6A provides $X_c(t)$ versus ln time at 240 °C for sPS OMMT mixtures. The same general trend of an increase in the time required for crystallization with increasing clay content is observed with sPS OMMT as with sPS Na^+MMT (Fig. 5A). It is likely that the increase in the time required for crystallization using the organically-modified montmorillonite in the sPS matrix may be attributed to the rejection OMMT particles from the crystalline domains as crystallization proceeds [49].

The effect of incorporating organically-modified MMT on the crystallization behavior of SsPS is shown in Fig. 6B. In profound contrast to sPS OMMT samples, there is a drastic reduction in the time required for the material to crystallize with increasing concentrations of OMMT. This behavior indicates that OMMT platelets may impart a nucleating effect during isothermal crystallization of the SsPS. Coupling this observation with morphological observations from WAXD and TEM analyses, we find that rate of

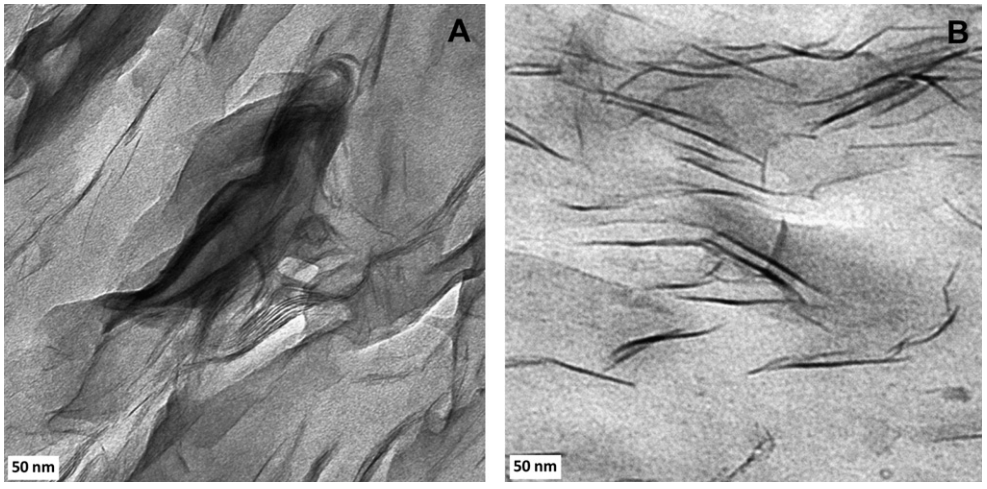

Fig. 4. TEM of (A) sPS 5 wt.% OMMT mixtures and (B) SsPS 5 wt.% OMMT mixtures. The scale bar in each image is 50 nm.

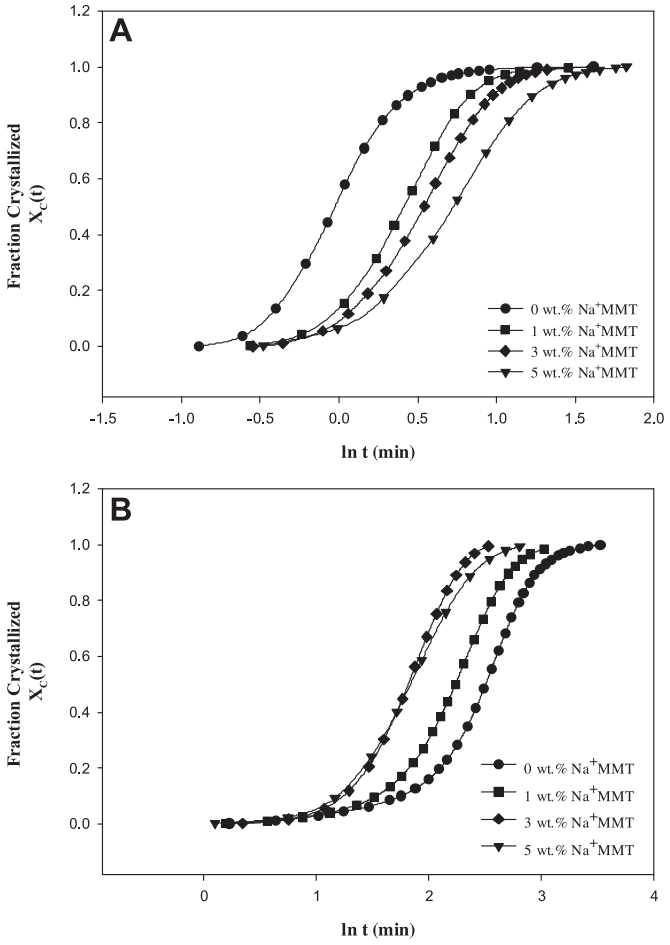

Fig. 5. $X_c(t)$ versus ln time at 240 °C for (A) sPS Na^+MMT mixtures and (B) SsPS Na^+MMT mixtures.

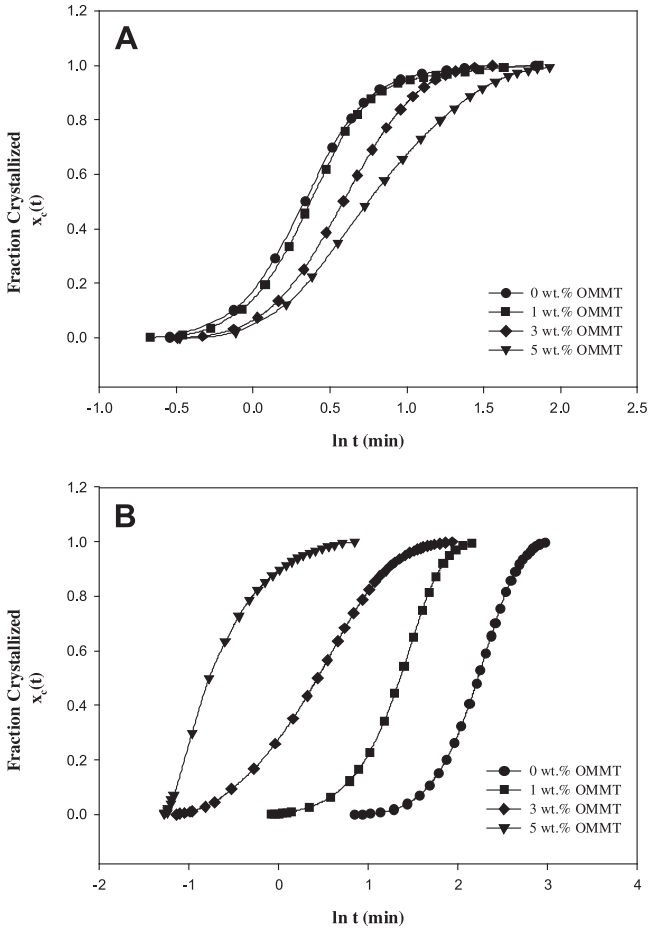

Fig. 6. $X_c(t)$ versus ln time at 240 °C for (A) sPS OMMT mixtures and (B) SsPS OMMT mixtures.

crystallization increases with the degree of exfoliation of clay platelets within the SsPS matrix.

A kinetic evaluation of the crystallization behavior of sPS and SsPS mixtures was completed using the Avrami approach [50–52]. The Avrami equation is given in equation (2) and is used to determine the extent of fractional crystallinity, $X_c(t)$ at time t.

$$X_c(t) = 1 - \exp(-Kt)^n \quad (2)$$

The Avrami rate constant is represented by K and n is the Avrami exponent. The Avrami exponent, n, provides insight into the type of nucleation and growth that occurs within the system. The kinetic analysis of the isothermal crystallization behavior of the polymer clay hybrids is done utilizing the Avrami equation in the following form:

$$\ln[-\ln(1 - X_c(t))] = n \ln t + \ln K \quad (3)$$

The linear portions of the graphs in Figs. 5 and 6 where $X_c(t) = 0.3$ to 0.7 were used to construct plots of ln[-ln(1- Xc(t))] versus ln t where n and K were obtained from the slope and intercept, respectively.

Table 1 summarizes the kinetic parameters obtained for isothermal crystallization processes at 240 °C. For sPS Na^+MMT and OMMT mixtures, the Avrami exponent n remains between values of $n = 3.42–2.60$. Avrami exponents within this range suggest a three dimensional spherical growth process and there is no significant change in the dimensionality of the crystalline superstructure with the type of clay incorporated into the sPS matrix. The Avrami rate constants K provided in Table 1 decrease and $t_{½}$ values (Fig. 7) increase with increasing clay content for sPS Na^+MMT and OMMT mixtures. The decrease in K and increase in the $t_{½}$ values correspond to slower crystallization rates upon incorporation of increasing

Table 1
Kinetic Parameters for sPS and SsPS Clay Mixtures at 240 °C.

Polymer Clay System	n	K (min^{-1})
sPS wt.% Na^+MMT		
0	3.39	7.3×10^{-1}
1	3.25	1.8×10^{-1}
3	3.09	1.3×10^{-1}
5	2.67	9.7×10^{-2}
SsPS wt.% Na^+MMT		
0	3.49	5.4×10^{-4}
1	2.71	1.6×10^{-3}
3	2.96	3.0×10^{-3}
5	3.62	7.1×10^{-3}
sPS wt.% OMMT		
0	3.26	2.2×10^{-1}
1	3.42	1.8×10^{-1}
3	3.02	1.1×10^{-1}
5	2.60	9.7×10^{-2}
SsPS wt.% OMMT		
0	3.03	8.1×10^{-4}
1	2.84	1.5×10^{-2}
3	1.71	3.3×10^{-1}
5	2.42	3.8×10^{-1}

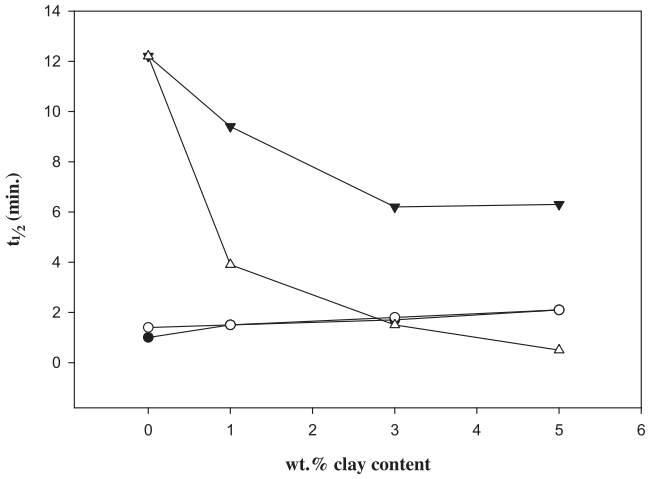

Fig. 7. Crystallization half-time versus wt.% clay content. Closed circles – sPS Na^+MMT, open circles - sPS OMMT, closed triangles – SsPS Na^+MMT, and open triangles – SsPS OMMT.

amounts of clay into the sPS matrix. This suggests that the poorly dispersed clay tactoids within the sPS matrix are not effective as nucleating agents, and may inhibit crystal growth due to an increase in melt viscosity [49,53].

For the SsPS Na^+MMT mixtures (Table 1), the Avrami exponent n ranges from a value of $n = 3.62$ to 2.71, indicating three dimensional spherical growth during isothermal crystallization at 240 °C. The $t_{½}$ values of SsPS Na^+MMT mixtures as shown in Fig. 7 decrease with increasing Na^+MMT concentration, and the Avrami rate constant K increases (Table 1) suggesting that SsPS crystallizable chain segments gain additional mobility as more clay is added to the system, and/or the clay increases nucleation.

For SsPS containing organically-modified montmorillonite, the Avrami exponents are indicative of three dimensional spherical growth as well (Table 1). The Avrami rate constant K increases (Table 1) and $t_{½}$ values for SsPS are significantly reduced upon successive increases in OMMT concentration as shown in Fig. 7. It is also important to note that the $t_{½}$ value for SsPS 5 wt.% OMMT is 0.5 min and is now on the same timescale of crystallization as pristine sPS with a $t_{½}$ value of 1.0 min.

The reduction in the crystallization half-time of SsPS clay mixtures is opposite to the behavior displayed by sPS clay mixtures which exhibit increased crystallization half-times upon incorporating clay into sPS homopolymer matrix. The more pronounced changes in the crystallization behavior of the SsPS ionomer in the presence of the clay are likely due to the disruption of the physical crosslinks of the ionic aggregates leading to higher nucleation, more chain mobility, and thus more rapid crystallization.

Based upon both the morphological analysis provided from WAXD and TEM in addition to the crystallization studies, we attribute the enhanced crystallization behavior of SsPS nanocomposites to a number of complex interrelated phenomena including disruption of the ionomer electrostatic network, a plasticization effect by the presence of the clay surfactant in the SsPS OMMT nanocomposites, and a nucleation effect due to exfoliated clay platelets in SsPS OMMT. The mechanistic origins of increased crystallization rates in SsPS ionomer clay nanocomposites are likely the result of multiple phenomena that encompass highly-specific mechanisms that are unique to ionomers and more general behaviors that are observed in many polymer composite systems.

Ionomer properties that may be significantly altered in the presence of aluminosilicate platelets include the stability of ionic aggregates that are formed through electrostatic interactions between dipoles consisting of negatively charged sulfonate groups and positively charged neutralizing cations. A disruption of the electrostatic interactions in these ionomers leads to a destabilization of the electrostatic physically-crosslinked network thereby greatly increasing the mobility of crystallizable polymer chains that were previously constrained. More specifically, the interaction of ionomer chains with the layered silicate surface may occur in primarily three ways: interaction of the negatively charged sulfonate groups with positively charged edges of clay platelets, cation exchange of ionomer Cs^+ counterions with Na^+ ions of pristine Na^+MMT and quaternary amine counterions of the organically-modified polymer, and possible hydrophobic interactions of ionomer chains with the long chain alkyl moieties provided by the clay organic modification agent in the SsPS OMMT [36].

Chisholm [24] and Barber [25] proposed a two-stage model based on polyester ionomer clay nanocomposites that attributed the formation of highly exfoliated morphologies to the interaction of the negatively charged sulfonate groups with the positively charged edges of the aluminosilicate platelet. This initial site of ionomer attachment to the clay platelet edge thereby facilitates the movement of mobile polymer chains into the intergallery spacing. Although slightly slower crystallization rates were observed for PET ionomer clay containing nanocomposites, this proposed mechanism of ionomer clay interaction may still provide a plausible mechanism for potential interactions between the SsPS ionomer nanocomposites.

Govindaiah and coworkers [37] suggested, in their study of SsPS nanocomposites, that an increase in the surface energy of sPS through the incorporation of polar entities allows increased interactions between the polymer matrix and the clay surface. However, crystallization data obtained within this study suggests that changes in the surface energy of the polymer alone may not be the sole mechanism by which the crystallization behavior of SsPS is altered. The possibility of a plasticization effect contributed by the clay surfactant must also be considered. Orler and coworkers [36] studied the incorporation of ionic surfactants and nonpolar plasticizers into lightly sulfonated sPS. A slight increase in the crystallization rate of SsPS was observed when nonpolar plasticizers were added to lightly sulfonated sPS. The increase in the rate of crystallization using the polar surfactant was attributed to preferential plasticization of the surfactant into the ionomer aggregate-rich cluster phases and the matrix phase as well [54]. It is also possible that the hydrocarbon tail of the OMMT surfactant may plasticize the sPS rich phase thus providing additional molecular mobility to sPS chains within the matrix phase. However, the large reduction in the rate of crystallization in SsPS OMMT nanocomposites may be more directly related to potential interaction with the quaternary amine headgroup component of the clay surfactant and the ionomer styrenesulfonate groups. As a control, we prepared SsPS ionomer mixtures containing an equivalent amount of organic modification agent (DMHTB) that is present in samples containing 1, 3, or 5 wt.% of organically-modified montmorillonite clay. At maximum loading (equivalent to 5 wt.% clay) the crystallization half-time of the SsPS ionomer containing only the DMHTB surfactant decreases by a factor of 2 compared to the pure SsPS ionomer. This reduction in the crystallization half-time is attributed to the preferential plasticization by the clay surfactant resulting in a destabilization of the electrostatic network, and thus greater mobility of crystallizable SsPS segments. In contrast, the SsPS ionomer containing the clay that has been organically-modified with the DMHTB surfactant exhibits much smaller $t_{½}$ values that decrease by a factor of 25 relative to the pure SsPS ionomer. Thus, given the relatively minor effect of the free surfactant, these data suggest that the well-exfoliated clay platelets present within the SsPS ionomer matrix act as nucleation sites and thereby increase the overall rate of bulk crystallization.

Polarized light microscopy was used to investigate the effect of the pristine and organically-modified clay on the spherulitic growth rates of the sPS homopolymer and the SsPS ionomer. Fig. 8A shows the plot of spherulite radius versus time for the pure sPS homopolymer and the homopolymer containing 3 wt.% Na^+MMT and OMMT under isothermal crystallization conditions at 240 °C. From this plot, it is clear that the spherulitic growth rate of the sPS homopolymer does not change upon incorporation of clay. The spherulitic growth rates for pure sPS and both clay containing sPS composites remain at 32 μm/min as listed in Table 2. However, it can be seen from the plot of spherulite radius versus time of the pure SsPS ionomer and the SsPS ionomer containing 3 wt.% Na^+MMT in Fig. 8B that there is a large increase in the spherulitic growth rate of SsPS upon incorporation of 3 wt.% Na^+MMT. The spherulitic growth rate of the pure SsPS ionomer increases from 1.6 μm/min to 10.3 μm/min with the addition of 3 wt.% Na^+MMT. Upon incorporation of 3 wt.% of organically-modified clay, the SsPS spherulitic growth rate is so rapid under isothermal crystallization at 240 °C that a growth rate could not be measured. Such a dramatic increase in the spherulitic growth of SsPS in the presence of both pristine and organically-modified clay strongly suggests that the presence of exfoliated clay platelets leads to a destabilization of the electrostatic network allowing more rapid nucleation and growth of the crystalline domains.

Polarized light microscopy provides a very local view of the crystalline structure for a small portion of the sample and may not necessarily be representative of the entire sample. SALLS allows a more global assessment of the crystalline superstructure to be obtained and an average spherulite size to be determined. Therefore, SALLS was used in order to determine the effect of incorporation of clay on the spherulite size [55–58] and nucleation density [59,60] of the sPS homopolymer and the SsPS ionomer.

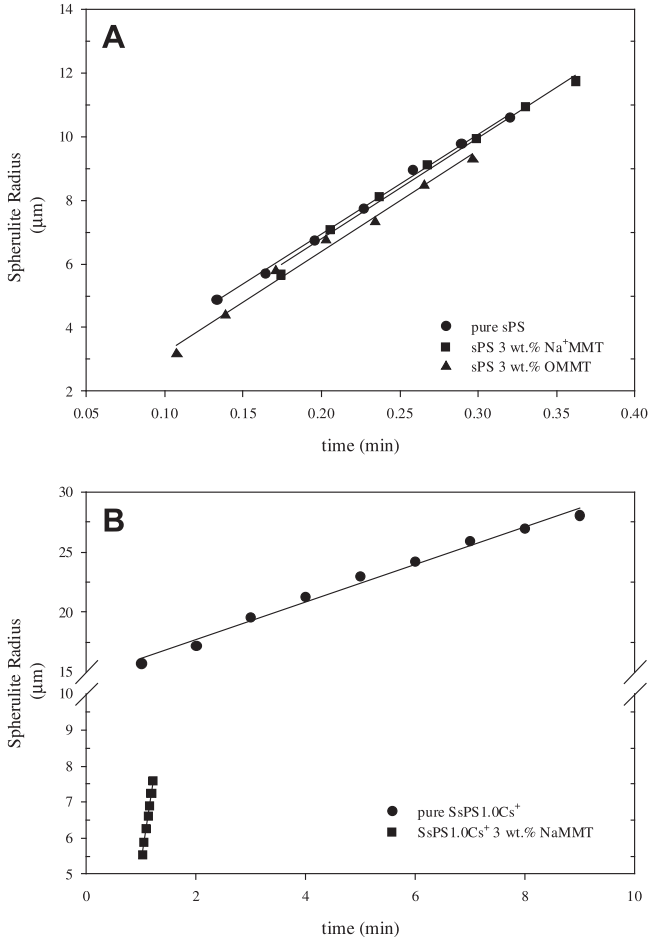

Fig. 8. Spherulite radius versus time of (A) pure sPS and sPS containing 3 wt. % of Na^+MMT and OMMT clay and (B) of pure SsPS and SsPS containing 3 wt.% Na^+MMT.

Table 2
Spherulitic Growth Rate, Spherulite Diameter, and Nucleation Density for sPS and SsPS Clay Mixtures.

Polymer Clay System	Spherulitic Growth Rate (μm/min)	Spherulite Diameter (μm)	Nucleation Density (sites/μm^3)
Pure sPS	32	98.9	1.9×10^{-5}
sPS 3 wt.% Na^+MMT	32	70.7	5.3×10^{-5}
sPS 3 wt.% OMMT	32	59.2	9.1×10^{-5}
Pure SsPS	1.6	71.2	5.2×10^{-5}
SsPS 3 wt.% Na^+MMT	10	55.0	1.1×10^{-4}
SsPS 3 wt.% OMMT	–	38.0	3.4×10^{-4}

Fig. 9A through Fig. 9C shows the SALLS patterns of the sPS homopolymer, sPS 3 wt.% Na^+MMT, and sPS 3 wt.% OMMT, respectively. The SALLS patterns of SsPS, SsPS 3 wt.% Na^+MMT, and SsPS 3 wt.% OMMT are provided in Fig. 9D through Fig. 9F, respectively. Upon comparing the SALLS patterns for the pure sPS and SsPS materials, it can be seen that the pure matrices consist of well-defined four-leaf-clover patterns under H_v mode. However in contrast, the SALLS patterns of sPS and SsPS nanocomposites are diffuse four-leaf-clover patterns. The more diffuse clover-leaf patterns for the clay containing matrices are attributed to the development of more irregular (less organized) spherulites due to the inclusion of clay particles inside the spherulites. Similar SALLS patterns have been observed for many different polymer clay nanocomposites systems such as nylon [61], low-density polyethylene [62], polypropylene [63], polylactide [64], PVDF [58], and poly[(butylene succinate)]-co-adipate] [65].

The most significant observation from the SALLS patterns is the difference in spherulite diameter between the homopolymer and ionomer matrices containing clay. The average spherulite size was determined using the following relationship [42]:

$$2\pi\frac{D}{\lambda}\sin\frac{\theta}{2} = 4.1 \tag{4}$$

The spherulite diameters for the different materials are provided in Table 2. Generally, there is a decrease in size of the spherulite upon incorporation of clay in both the sPS homopolymer and the SsPS ionomer.

SALLS can also be used to determine the average primary nucleation density, N, using equation (5) shown below where D_m is the average diameter of the spherulite prior to impingement.

$$N = \left(\frac{3}{4}\pi\right)\left(\frac{D_m}{2}\right)^{-3} \tag{5}$$

D_m is determined using equation (4). The smaller spherulite size and higher nucleation density of pure SsPS compared to pure sPS (Table 2) may be attributed to the presence of ionic aggregates within SsPS that decrease polymer chain mobility [35]. During the crystallization of SsPS, the dynamic electrostatic network restricts the mobility of the crystallizable chain segments leading to more effective nucleation, but slower growth. As shown in Table 2, the nucleation densities for sPS and SsPS increase upon incorporation of both pristine and organically-modified clay. However, there is a more pronounced increase in the nucleation density of the SsPS clay containing mixtures compared to that of the sPS clay containing mixtures. The profound increase in the nucleation density

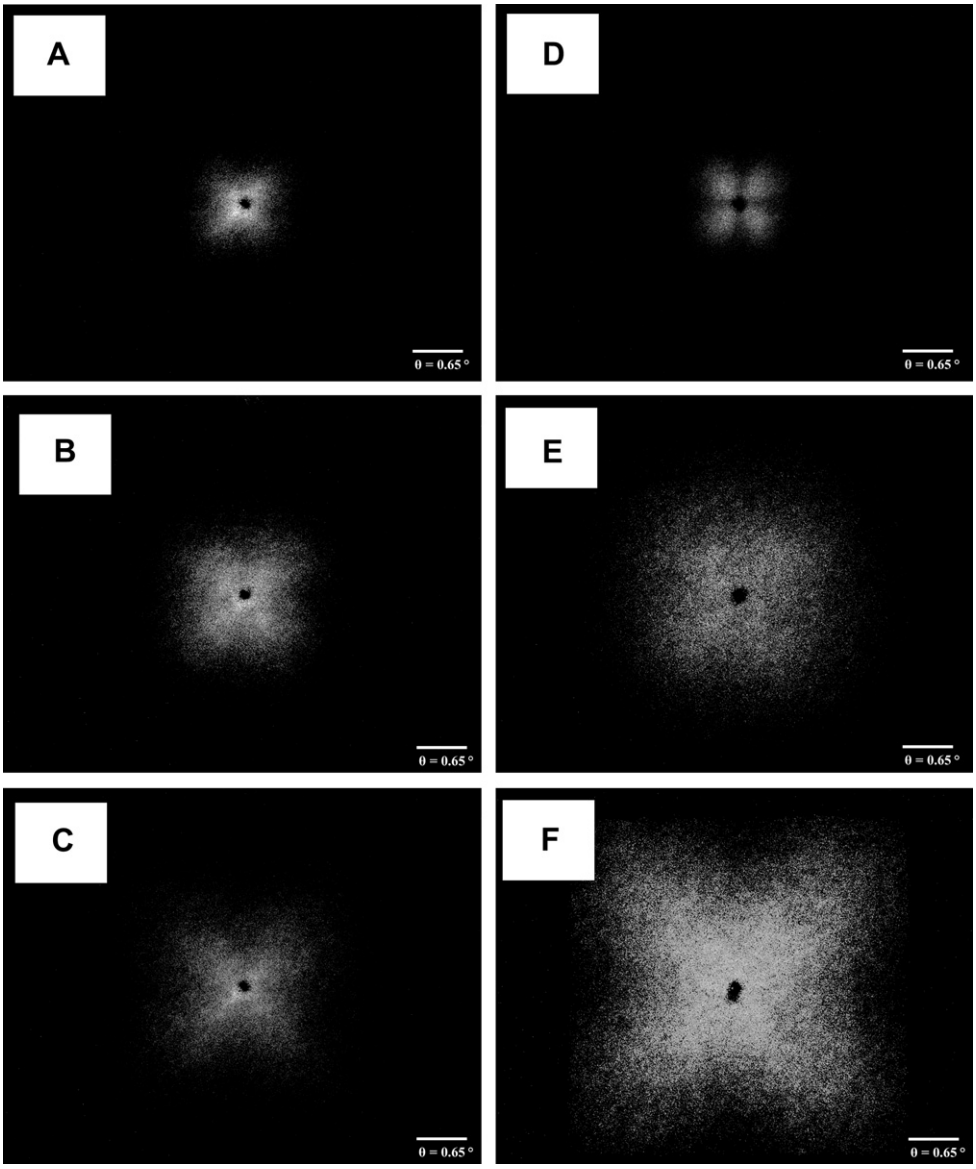

Fig. 9. H_v SALLS patterns of (A) pure sPS (B) sPS 3 wt.% Na^+MMT (C) sPS 3 wt.% OMMT (D) pure SsPS (E) SsPS 3 wt.% Na^+MMT and (F) SsPS 3 wt.% OMMT.

of the SsPS clay containing mixtures is attributed to improved exfoliation and dispersion of the clay platelets within the lightly sulfonated sPS ionomer matrix, which disrupts the electrostatic network through enhanced in ionomer/clay interactions. The improved exfoliation and dispersion of clay platelets within the SsPS ionomer compared to that of the pure sPS homopolymer is clearly shown in Figs. 1–4.

4. Conclusion

We have utilized the solution intercalation technique to prepare polymer clay mixtures using sPS and SsPS. The study shows the significant morphological differences between polymer clay mixtures prepared using the sPS homopolymer and the sulfonated sPS copolymer using WAXD and TEM analyses. The morphology of SsPS OMMT mixtures consist of a well-dispersed, primarily exfoliated morphology exhibiting single platelet features and stacks consisting of tens of platelets. In contrast, sPS OMMT hybrids appeared to consist of a highly mixed morphology dominated by the presence of micron-scale aggregates of clay along with smaller scale morphological features including intercalated platelets and single platelets as well. Both sPS and SsPS MMT hybrids revealed large agglomerates of pristine clay with no evidence of significant degrees of intercalation or exfoliation present. The improvement in the degree of intercalation/exfoliation in both sPS and SsPS OMMT mixtures is attributed to enhanced polymer clay interactions due to the presence of the clay organic modification agent that imparts hydrophobicity to the naturally hydrophilic clay platelets.

Utilization of SsPS as a model ionomer to study the effect of clay on the crystallization of behavior semicrystalline ionomers has shown that the rate of crystallization is significantly increased in both tactoid and exfoliated SsPS clay morphologies. The crystallization half-time for the neat SsPS ionomer is 12.2 min, while the $t_{½}$ value decreases to 9.2 and 0.5 min for the SsPS ionomer containing 5 wt.% Na^+MMT and OMMT respectively. The crystallization half-time of the SsPS ionomer is reduced to a greater degree in the presence of organically-modified clay versus pristine Na^+MMT. It is likely that the more rapid rate of crystallization of SsPS in the

presence of OMMT is due to exfoliated, well-dispersed platelets and a complex combination of disruption of the electrostatic network, plasticization effects due to the clay surfactant, and nucleation effects due to the presence of the platelets. We have found that unlike sulfonated PBT nanocomposites [24], the rate of crystallization of SsPS nanocomposites may be dependent upon the degree of exfoliation as observed in studies of sulfonated PET nanocomposites [25].

Acknowledgements

The authors gratefully acknowledge the financial support of Proctor & Gamble through the Proctor & Gamble Industrial Polymer Science Graduate Fellowship Award. This work was supported partially by the Major Research Instrumentation program of the National Science Foundation under the Award No. MRI 0421406 and by the National Science Foundation CBET-0756439 grant.

References

[1] Alexandre M, Dubois P. Materials Science and Engineering: R: Reports 2000;28(1–2):1–63.
[2] Sinha Ray S, Okamoto M. Progress in Polymer Science 2003;28(11):1539–641.
[3] Manias E, Touny A, Wu L, Strawhecker K, Lu B, Chung TC. Chemistry of Materials 2001;13(10):3516–23.
[4] Galgali G, Ramesh C, Lele A. Macromolecules 2001;34(4):852–8.
[5] Wang S, Hu Y, Zhongkai Q, Wang Z, Chen Z, Fan W. Materials Letters 2003;57(18):2675–8.
[6] Durmus A, Kasgoz A, Macosko CW. Polymer 2007;48(15):4492–502.
[7] Calcagno CIW, Mariani CM, Teixeira SR, Mauler RS. Polymer 2007;48(4):966–74.
[8] Wan T, Chen L, Chua YC, Lu X. Journal of Applied Polymer Science 2004;94(4):1381–8.
[9] Acierno D, Scarfato P, Amendola E, Nocerino G, Costa G. Polymer Engineering and Science 2004;44(6):1012–8.
[10] Li X, Kang T, Cho WJ, Lee JK, Ha CS. Macromolecular Rapid Communications 2001;22(16):1306–12.
[11] Cho JW, Paul DR. Polymer 2001;42(3):1083–94.
[12] Mathias LJ, Davis RD, Jarrett WL. Macromolecules 1999;32(23):7958–60.
[13] Sorrentino A, Pantani R, Brucato V. Polymer Engineering & Science 2006;46(12):1768–77.
[14] Park CI, Kim MH, Ok Park O. Polymer 2004;45(4):1267–73.
[15] Wu TM, Hsu SF, Chien CF, Wu JY. Polymer Engineering and Science 2004;44(12):2288–97.
[16] Tseng CR, Wu SC, Wu JJ, Chang FC. Journal of Applied Polymer Science 2002;86(10):2492–501.
[17] Wu TM, Hsu SF, Wu JY. Journal of Polymer Science Part B: Polymer Physics 2003;41(6):560–70.
[18] Kim MH, Park CI, Choi WM, Lee JW, Lim JG, Park OO, et al. Journal of Applied Polymer Science 2004;92(4):2144–50.
[19] Bruzaud S, Grohens Y, Ilinca S, Carpentier J-F. Macromolecular Materials and Engineering 2005;290(11):1106–14.
[20] Torre L, Lelli G, Kenny JM. Journal of Applied Polymer Science 2006;100(6):4957–63.
[21] Wu HD, Tseng CR, Chang FC. Macromolecules 2001;34(9):2992–9.
[22] Tseng C-R, Lee H-Y, Chang F-C. Journal of Polymer Science Part B: Polymer Physics 2001;39(17):2097–107.
[23] Park CI, Choi WM, Kim MH, Park OO. Journal of Polymer Science Part B: Polymer Physics 2004;42(9):1685–93.
[24] Chisholm BJ, Moore RB, Barber G, Khouri F, Hempstead A, Larsen M, et al. Macromolecules 2002;35(14):5508–16.
[25] Barber GD, Calhoun BH, Moore RB. Polymer 2005;46(17):6706–14.
[26] Sánchez-Valdes S, López-Quintanilla ML, Ramírez-Vargas E, Medellín-Rodríguez FJ, Gutierrez-Rodriguez JM. Macromolecular Materials and Engineering 2006;291(2):128–36.
[27] Shah RK, Paul DR. Macromolecules 2006;39(9):3327–36.
[28] Bhiwankar NN, Weiss RA. Polymer 2006;47(19):6684–91.
[29] Shah RK, Paul DR. Polymer 2006;47(11):4075–84.
[30] Bhiwankar NN, Weiss RA. Polymer 2005;46(18):7246–54.
[31] Shah RK, Kim DH, Paul DR. Polymer 2007;48(4):1047–57.
[32] Shah RK, Hunter DL, Paul DR. Polymer 2005;46(8):2646–62.
[33] Orler EB, Calhoun BH, Moore RB. Macromolecules 1996;29(18):5965–71.
[34] Orler EB, Yontz DJ, Moore RB. Macromolecules 1993;26(19):5157–60.
[35] Orler EB, Moore RB. Macromolecules 1994;27(17):4774–80.
[36] Orler EB, Gummaraju RV, Calhoun BH, Moore RB. Macromolecules 1999;32(4):1180–8.
[37] Govindaiah P, Mallikarjuna SR, Ramesh C. Macromolecules 2006;39(21):7199–203.
[38] Ghosh AK, Woo EM. Polymer 2004;45(14):4749–59.
[39] Robello DR, Yamaguchi N, Blanton T, Barnes C. Journal of the American Chemical Society 2004;126(26):8118–9.
[40] Ryu JG, Kim H, Lee JW. Polymer Engineering and Science 2004;44(7):1198–204.
[41] Chen K, Wilkie CA, Vyazovkin S. The Journal of Physical Chemistry B 2007;111(44):12685–92.
[42] Stein RS, Rhodes MB. Journal of Applied Physics 1960;31(11):1873–84.
[43] Vittoria V, De Candia F, Iannelli P, Immirzi A. Die Makromolekulare Chemie Rapid Communications 1988;9(11):765–9.
[44] De Candia F, Carotenuto M, Guadagno L, Vittoria V. Journal of Macromolecular Science, Part B: Physics 1996;35(2):265–75.
[45] Tashiro K, Ueno Y, Yoshioka A, Kobayashi M. Macromolecules 2000;34(2):310–5.
[46] Doh JG, Cho I. Polymer Bulletin 1998;41(5):511–8.
[47] LeBaron PC, Wang Z, Pinnavaia TJ. Applied Clay Science 1999;15(1–2):11–29.
[48] Zhang W, Chen D, Zhao Q, Fang Y. Polymer 2003;44(26):7953–61.
[49] Martuscelli E. Polymer Engineering & Science 1984;24(8):563–86.
[50] Avrami M. The Journal of Chemical Physics 1939;7(12):1103–12.
[51] Avrami M. The Journal of Chemical Physics 1940;8(2):212–24.
[52] Avrami M. The Journal of Chemical Physics 1941;9(2):177–84.
[53] Hotta S, Paul DR. Polymer 2004;45(22):7639–54.
[54] Kim JS, Roberts SB, Eisenberg A, Moore RB. Macromolecules 1993;26(19):5256–8.
[55] Ma D, Akpalu YA, Li Y, Siegel RW, Schadler LS. Journal of Polymer Science Part B: Polymer Physics 2005;43(5):488–97.
[56] Filippi S, Marazzato C, Magagnini P, Minkova L, Dintcheva NT, Mantia FPL. Macromolecular Materials and Engineering 2006;291(10):1208–25.
[57] Famulari A, Arosio P, Filippi S, Marazzato C, Magagnini P, Minkova L, et al. Journal of Macromolecular Science, Part B: Physics 2007;46(2):355–71.
[58] Patro TU, Mhalgi MV, Khakhar DV, Misra A. Polymer 2008;49(16):3486–99.
[59] Maiti P, Nam PH, Okamoto M, Hasegawa N, Usuki A. Macromolecules 2002;35(6):2042–9.
[60] Sinha Ray S, Yamada K, Okamoto M, Ogami A, Ueda K. Chemistry of Materials 2003;15(7):1456–65.
[61] Katoh Y, Okamoto M. Polymer 2009;50(19):4718–26.
[62] Xiao Z, Li Y, Ma D, Schadler LS, Akpalu YA. Journal of Polymer Science Part B: Polymer Physics 2006;44(7):1084–95.
[63] Nam PH, Maiti P, Okamoto M, Kotaka T, Hasegawa N, Usuki A. Polymer 2001;42(23):9633–40.
[64] Nam JY, Sinha Ray S, Okamoto M. Macromolecules 2003;36(19):7126–31.
[65] Sinha Ray S, Bandyopadhyay J, Bousmina M. European Polymer Journal 2008;44(10):3133–45.